Title

Sediment supply controls equilibrium channel geometry in gravel rivers

Journal

Proceedings of the National Academy of Sciences of the United States of America, 114(13)

ISSN

0027-8424

Authors

Pfeiffer, Allison M
Finnegan, Noah J
Willenbring, Jane K

Publication Date

2017-03-28

DOI

10.1073/pnas.1612907114

Peer reviewed

Sediment supply controls equilibrium channel geometry in gravel rivers

Allison M. Pfeiffer[a,1], Noah J. Finnegan[a], and Jane K. Willenbring[b]

[a]Department of Earth and Planetary Sciences, University of California, Santa Cruz, CA 95064; and [b]Scripps Institution of Oceanography, University of California, San Diego, CA 92037

Edited by Thomas Dunne, University of California, Santa Barbara, CA, and approved January 26, 2017 (received for review August 3, 2016)

In many gravel-bedded rivers, floods that fill the channel banks create just enough shear stress to move the median-sized gravel particles on the bed surface (D_{50}). Because this observation is common and is supported by theory, the coincidence of bankfull flow and the incipient motion of D_{50} has become a commonly used assumption. However, not all natural gravel channels actually conform to this simple relationship; some channels maintain bankfull stresses far in excess of the critical stress required to initiate sediment transport. We use a database of >300 gravel-bedded rivers and >600 ^{10}Be-derived erosion rates from across North America to explore the hypothesis that sediment supply drives the magnitude of bankfull shear stress relative to the critical stress required to mobilize the median bed surface grain size (τ^*_{bf}/τ^*_c). We find that τ^*_{bf}/τ^*_c is significantly higher in West Coast river reaches (2.35, n = 96) than in river reaches elsewhere on the continent (1.03, n = 245). This pattern parallels patterns in erosion rates (and hence sediment supplies). Supporting our hypothesis, we find a significant correlation between upstream erosion rate and local τ^*_{bf}/τ^*_c at sites where this comparison is possible. Our analysis reveals a decrease in bed surface armoring with increasing τ^*_{bf}/τ^*_c, suggesting channels accommodate changes in sediment supply through adjustments in bed surface grain size, as also shown through numerical modeling. Our findings demonstrate that sediment supply is encoded in the bankfull hydraulic geometry of gravel bedded channels through its control on bed surface grain size.

river channel geometry | sediment supply | sediment transport

What determines the shape of alluvial rivers? These self-formed channels emerge through the interaction of flowing water and transported sediment. Explaining widely observed trends in river channel hydraulic geometry remains an ongoing challenge in the field of geomorphology. Gravel-bedded alluvial rivers (whose bed and banks comprise sediment transported by the river) approach equilibrium geometry through feedbacks between deposition, erosion, and bed surface armoring as well as through channel slope change (1–3). These responses in channel geometry and surface grain size accommodate perturbations in the water and sediment supply regimes. Thus, sediment supply is among the key controls on the morphology of all river channels, and understanding linkages between sediment supply and channel morphology is a central question in much of fluvial geomorphology, civil engineering, and river restoration.

Decades of observations in gravel-bedded alluvial channels support the pervasiveness of threshold channels (4–6) in which the channel dimensions adjust such that the threshold for motion of the median bed surface grain size (D_{50}) occurs at, or just below, bankfull flow. These observations are reinforced by theoretical work (7) showing that, at bankfull flow, a straight channel with noncohesive banks will maintain a stable channel width with a shear stress in the center of the channel that just exceeds that required to move the median-sized grains on the bed surface.

The seeming ubiquity of threshold channels provides a convenient constraint on gravel-bedded river morphology, suggesting that the near equivalence of the stress required for sediment motion (critical Shields stress, τ^*_c) and the mean bankfull bed stress (τ^*_{bf}) may be a criterion to which all gravel rivers must conform (8). The critical Shields stress (τ^*_c) describes the amount of stress needed to initiate median grain motion, normalized for the grain size, and is generally between 0.03 and 0.08 (9). The bankfull Shields stress (τ^*_{bf}) describes the stress acting on the bed during bankfull flow, and (at the reach scale) is approximated as

$$\tau^*_{bf} = \rho R_{bf} S / (\rho_s - \rho) D_{50}, \quad [1]$$

where ρ is the density of water (1,000 kg/m^3), ρ_s is the density of sediment, R_{bf} is the bankfull hydraulic radius, and S is the channel slope (note that all Shields stresses referred to herein apply to D_{50}).

However, the orders of magnitude global variability in basin-wide erosion rates (and hence sediment yields) (10) points to a potential problem with widespread application of a threshold channel model. In tectonically active settings, channels, as the primary conduits of material off the landscape, must be adjusted to move high sediment loads. The sediment transport capacity of a channel is often modeled as a function of the excess stress, or difference between the bankfull and critical stress (τ^*_{bf}-τ^*_c) (11). Consequently, all else being equal, it would seem that higher bankfull stresses are needed to transport large volumes of material in tectonically active settings. The requirement to transport a high sediment supply ($\tau^*_{bf} > \tau^*_c$) is seemingly at odds with the threshold channel assumption ($\tau^*_{bf} \approx \tau^*_c$).

Previous work has hinted at a relationship between sediment supply and τ^*_{bf}/τ^*_c. The difference between the grain size predicted by rearranging Eq. **1** and observed grain size can theoretically be used to predict sediment supply (12), although this idea has yet to be validated with field data. Further, τ^*_{bf}/τ^*_c has been shown to

Significance

Geomorphologists commonly assume that gravel-bedded rivers tend toward a "threshold" equilibrium state, in which the median-sized grains on the riverbed surface begin to move at the bankfull flood stage. However, here we show that this widely held assumption fails to capture a more fundamental pattern in river channel geometry. Our findings provide evidence that river channel geometry and grain size are inherently linked to the supply of sediment transported from upstream. Threshold channels may therefore simply reflect settings with low sediment supplies, while high sediment supply channels are adjusted to transport large volumes of material during bankfull floods. Thus, an understanding of sediment supply is key to interpreting, predicting, and restoring bankfull geometry in rivers.

Author contributions: A.M.P. and N.J.F. designed research; A.M.P. and J.K.W. performed research; J.K.W. contributed new reagents/analytic tools; A.M.P. and N.J.F. analyzed data; and A.M.P. and N.J.F. wrote the paper.

The authors declare no conflict of interest.

This article is a PNAS Direct Submission.

[1]To whom correspondence should be addressed. Email: ampfeiff@ucsc.edu.

This article contains supporting information online at www.pnas.org/lookup/suppl/doi:10.1073/pnas.1612907114/-/DCSupplemental.

increase with decreasing bed stability (13), which is likely correlated with sediment supply. On the other hand, further confirmation of the ubiquity of threshold channels has continued to appear in the literature (8).

Although there is not a well-accepted link between sediment supply and τ^*_{bf}/τ^*_c, it is clear that sediment supply can affect many aspects of channel morphology. Rivers with very high sediment supply are often braided (2), and aggradation occurs when the sediment supply to a channel is in excess of the channel's capacity to transport that sediment (14). Additionally, the bed surface can armor through size selective transport in low supply conditions (1, 3), or the bed surface grain size can fine in response to high sediment supply (15). Despite the prevalence of these observations, we lack a coherent understanding of how these responses are expressed in τ^*_{bf}, which is a function of both grain size and channel geometry. Although it is clear that sediment supply impacts channel morphology, this does not necessarily translate to an impact on τ^*_{bf}/τ^*_c. One can imagine that a river channel might respond to an increase in sediment supply through a decrease in bed surface armoring (reducing surface D_{50}) while maintaining a constant, threshold τ^*_{bf}/τ^*_c value through a concurrent decrease in S or R_{bf}, via widening. It could also be the case that a river channel would respond to an increase in sediment supply through a reduction in bed surface armoring without a change in channel geometry, yielding an increased τ^*_{bf}/τ^*_c. Here, we address the question, Do all gravel-bedded rivers, regardless of sediment supply, tend toward an equilibrium that maintains threshold conditions, or can τ^*_{bf}/τ^*_c vary with sediment supply?

To the extent that we understand and restore rivers according to their sediment supply regime, a clearer understanding of the relationship between sediment supply, bed surface grain size, and the hydraulic geometry of river channels is needed. A unifying model should explain both the widespread observation of threshold channels and the need for channels in tectonically active areas to transport large coarse sediment loads. Here we adopt and test the hypothesis that the balance between bankfull shear stress and bed surface grain size reflects not only the need to initiate sediment motion, as is commonly argued, but also the requirement that channels convey the load supplied from upstream (12).

To explore the controls on bed surface grain size and bankfull hydraulic geometry, and their relationship to sediment supply, we compiled a dataset of D_{50} and hydraulic geometry for 341 reaches of gravel-bedded rivers in North America (Fig. 1*A* and Dataset S1). Using these data, we explore patterns in τ^*_{bf} across the continent. Channel geometry and grain size reflect basin lithology, large wood loading, landslide history, land use history, hydrology, and relative roughness, among other factors; rather than attempting to control for all of these factors in a small subset of drainages, we take a continent-wide approach to addressing this problem. By gathering a large dataset across a wide variety of lithologies, climates, and land use histories, we gain sufficient statistical power to see past the "noise" that is inherent in such a compilation.

We compare patterns in τ^*_{bf}/τ^*_c to sediment supply, which we infer from an independent compilation of ^{10}Be-derived erosion rates from across North America (10, 16) (Fig. 1*D*) (*Materials and Methods*). The ^{10}Be erosion rates, which measure long-term ($\sim 10^3$ y) averages, are very often (17, 18) but not always (19, 20) in close agreement with short-term erosion rates. Also, the ratio of coarse sediment (which impacts gravel bed morphology) to fine sediment (which has no known bed-forming role in gravel-bed rivers) depends on lithology (21) and can vary widely between drainages and flood stages (22). With the understanding of these caveats, we proceed assuming that ^{10}Be erosion rates are a proxy for coarse (bedload) sediment supplied to a channel, and further address these assumptions in *Sediment Supply as a Driver of High* τ^*_{bf}/τ^*_c.

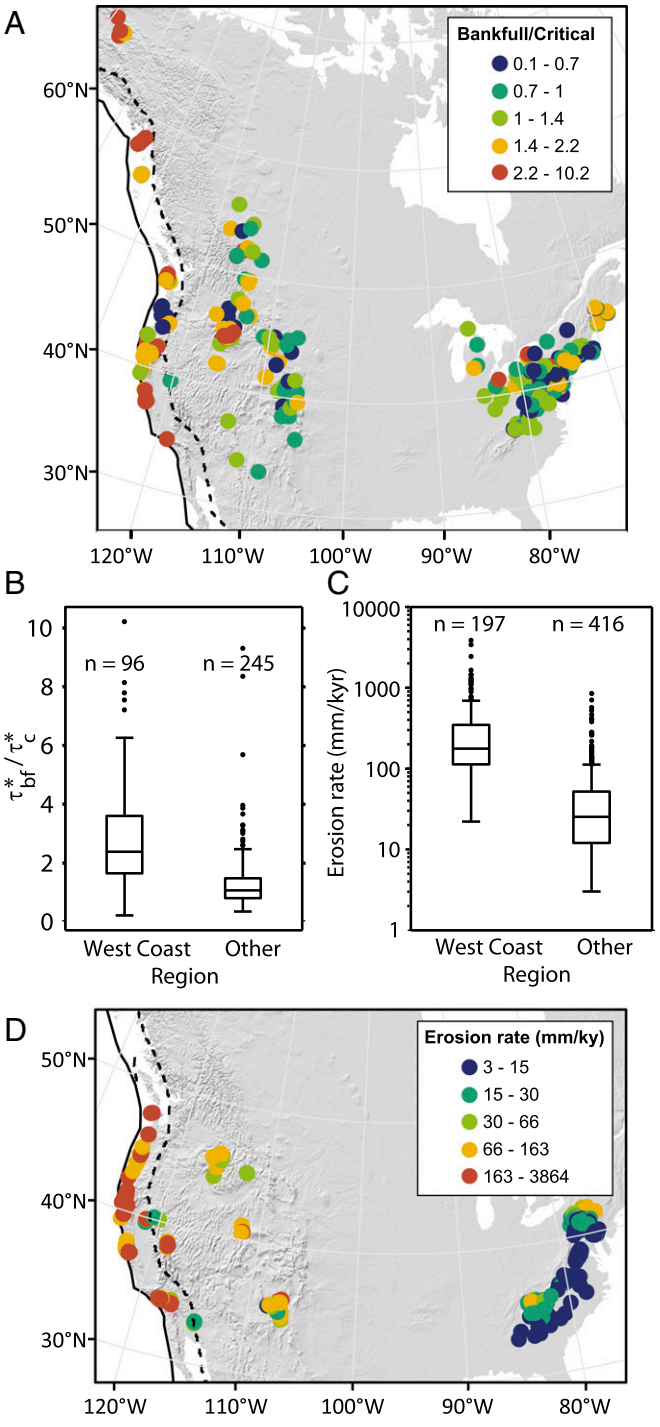

Fig. 1. Ratio of τ^*_{bf}/τ^*_c and ^{10}Be erosion rate data across North America. (*A*) Location of all hydraulic geometry sites in our data compilation. (*B* and *C*) Boxplots showing (*B*) the distribution of τ^*_{bf}/τ^*_c separated by region and (*C*) the distribution of ^{10}Be-derived erosion rates separated by region. (*D*) Location of ^{10}Be erosion rate sites in our data compilation. Solid line corresponds to the Pacific–North American Plate boundary used in this analysis (*Materials and Methods*). Dashed line marks the boundary between West Coast and Other sites. Data are separated into color bins by quintile.

Sediment Supply as a Driver of High τ^*_{bf}/τ^*_c

Calculating values of τ^*_c based on channel slope (23) (*Materials and Methods*), we find that the ratio of bankfull to critical Shields stress (τ^*_{bf}/τ^*_c) is significantly higher in West Coast rivers (median

$\tau^*_{bf}/\tau^*_c = 2.35$) than in other rivers ($\tau^*_{bf}/\tau^*_c = 1.03$, Welch's t test for unequal variance, $P = 3 \times 10^{-12}$) (Fig. 1*B*). This difference exists despite the wide spread in observed τ^*_{bf}/τ^*_c within both categories. The near equivalence of critical and bankfull Shields stress across most of the continent is in keeping with previous research (5, 7) and supports the threshold channel model. In contrast, the systematically high bankfull Shields stress in West Coast rivers has, to our knowledge, never been documented. Using depth, h, in place of R_{bf} in Eq. **1**, a common simplification (4, 24), results in only modest differences in τ^*_{bf}/τ^*_c (median "Other" = 1.12, "West Coast" = 2.81).

To test whether high sediment supply drives this pattern in hydraulic geometry, we estimate sediment transport capacity (*Materials and Methods*), which we compare with ^{10}Be-derived catchment-averaged erosion rates from across North America (10, 16). As with τ^*_{bf}/τ^*_c, ^{10}Be erosion rates are very statistically significantly higher ($P = 1.6 \times 10^{-14}$) on the West Coast (median E = 177 mm/ky) compared with the rest of the continent (E = 25 mm/ky, Fig. 1*C*). Normalizing both ^{10}Be-derived basin-wide erosion rate and sediment transport capacity (*Materials and Methods*) by their means, we find that sediment transport capacity and erosion rate decrease by about an order of magnitude moving east from the plate boundary (Fig. S1). These data suggest that more coarse sediment is being transported in regions with high sediment supply supporting our assertion that coarse sediment fluxes scale with ^{10}Be-derived catchment-averaged erosion rates.

Isolating the sites for which we have both ^{10}Be and channel geometry data (Dataset S2), we see that there is a statistically significant trend of increasing τ^*_{bf}/τ^*_c with increasing erosion rate (Fig. 2). This pattern persists in both long-term (^{10}Be) and short-term erosion rates. This consistency lends support to our assertion that ^{10}Be erosion rates are a valid proxy for coarse sediment supply at timescales relevant to channel adjustment. The assertion is further supported by recent work (18) showing that basins dominated by fluvial incision do not exhibit a time scale bias in erosion rates. The magnitude of variation in background erosion rates across the continent is substantially greater than the differences in sediment supply generally attributed to land use effects (20). In *Exploring Additional Explanations for High* τ^*_{bf}/τ^*_c, we discuss some of the factors that likely drive the scatter in Fig. 2. Because we do not know the error associated with the τ^*_{bf}/τ^*_c data, we cannot determine the slope of the true functional relationship between erosion rate and τ^*_{bf}/τ^*_c (25). Regressions (Fig. 2) represent a lower bound; τ^*_{bf}/τ^*_c is likely more sensitive to erosion rate than suggested in Fig. 2 (25).

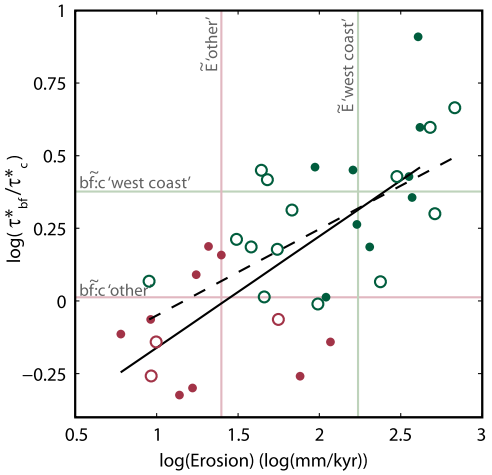

Fig. 2. Paired erosion and τ^*_{bf}/τ^*_c sites. The solid dots and solid line represent ^{10}Be erosion rates, and the open circles and dashed line represent short-term erosion rate measurements. West Coast data are in green; Other data are in maroon. See Dataset S2 for details on site pairings. There is a statistically significant relationship between erosion rate and τ^*_{bf}/τ^*_c, a relationship that holds true with both long-term ($P = 0.001$, $r^2 = 0.50$) and short-term ($P = 0.002$, $r^2 = 0.47$) erosion rates. The colored lines mark the median ^{10}Be erosion and τ^*_{bf}/τ^*_c values, color-coded by region.

We note that the least-squares fit to our paired sites data nearly crosses the intersection of the median erosion rate and τ^*_{bf}/τ^*_c for both the West Coast and Other populations. This finding suggests that the paired sites are representative of the larger data compilation. Thus, both continent-wide trends and paired sites suggest that rivers in high erosion rate landscapes, where sediment supplies are high, have adjusted to maintain high bankfull Shields stresses rather than maintaining threshold conditions at bankfull flow.

Sediment Supply Accommodated Through Armoring

The association between erosion rate and τ^*_{bf}/τ^*_c suggests that high sediment supply channels are some combination of deeper (greater bankfull depth), steeper (higher slope), and finer (smaller bed surface grain size) than their low sediment supply counterparts. Substantial work has been done connecting sediment supply conditions with bed surface armor ratio (D_{50}/D_{50ss}, where D_{50ss} is the median grain size of the subsurface) (1, 2, 12, 15). Although it is difficult to observe armoring of channels during high-flow conditions, the armor ratio of the channel measured at low flow appears to provide an index of the sediment supply and transport conditions during the formative flows (26–28). Bed surface armor forms through the selective transport of finer bed surface particles relative to coarser particles (29). In high sediment supply conditions, however, armor formation is reduced, leaving the bed surface more closely matching the grain size distribution of the subsurface (14). This connection between low armor ratio and high sediment supply suggests that high τ^*_{bf}/τ^*_c primarily results from bed surface fining.

Using subsurface grain size measurements available for a subset of our sites, we see that, indeed, armor ratio correlates with τ^*_{bf}/τ^*_c (Fig. 3). To more directly link armor ratio and sediment transport, we make estimates of instantaneous sediment transport capacity per unit width during bankfull flow, Q_t (square meters per second) (30) (*Materials and Methods*). Fig. 3 shows that the low armor ratio, high τ^*_{bf}/τ^*_c sites correspond with high estimated Q_t. This observation suggests that bed surface grain size adjusts in channels to transmit the high sediment load supplied during bankfull flow.

The above approach to predicting sediment transport capacity is simplified and limited by the data available to us; it is based solely on S, R_{bf}, and D_{50}. To independently validate the relationship between armor ratio, τ^*_{bf}/τ^*_c, and estimated Q_t, we examine the results of an independent sediment transport model (3) that explicitly incorporates the formation of armor and its effect on sediment transport in natural rivers (*Materials and Methods*). The physically based, empirically calibrated model evolves Q_t and armor ratio from an imposed bedload grain size distribution and Shields stress. Comparing the model output to our data compilation, we find good agreement with the general trends (Fig. 3): Both the independent model and the data from our compilation show decreasing armor ratio with increasing τ^*/τ^*_c and Q_t. This agreement points to the mechanistic relationship between sediment transport, armor ratio, and τ^*/τ^*_c. At formative flows, a high sediment supply equilibrium channel must maintain high sediment transport capacity, which is a function of τ^*_{bf}/τ^*_c (e.g., ref. 12). This high transport rate depresses armor formation. We observe these relationships in our data compilation (Fig. 3), and the mechanistic links are encoded in the model (3). That said, we acknowledge that there are limits to the effectiveness of bed surface armor in absorbing the effects of sediment

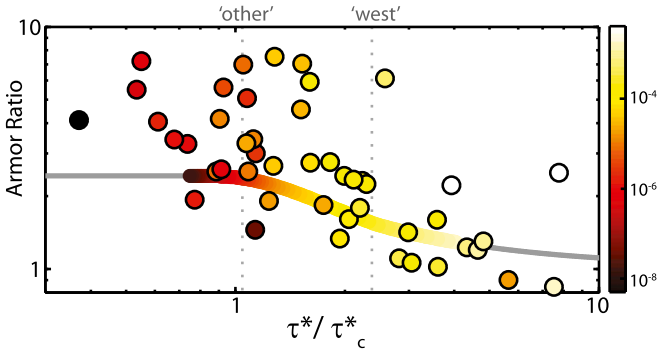

Fig. 3. Relationship between τ^*_{bf}/τ^*_c, armor, and sediment transport capacity. Points, which represent sites in our data compilation for which we have subsurface grain size measurements, are colored by predicted Q_t (30) (*Materials and Methods*). The solid line shows the relationship between armor ratio and τ^*/τ^*_c predicted using the Parker (3) model. The line is colored by predicted sediment transport capacity in the range of τ^*/τ^*_c for which the model was calibrated. The vertical dashed lines mark the median τ^*_{bf}/τ^*_c values in the West Coast and Other populations (Fig. 1*B*).

supply on τ^*_{bf}/τ^*_c. At some high sediment supply point, armor ratio approaches unity and bed surface aggradation begins (14).

Exploring Additional Explanations for High τ^*_{bf}/τ^*_c

Although our data support the idea that sediment supply is a significant driver of τ^*_{bf}/τ^*_c, other factors certainly influence this ratio. First, roughness elements such as immobile boulders or large in-channel wood can cause some of the total bankfull shear stress to be "partitioned" away from the bed (e.g., ref. 24). As a result of this form drag, the nondimensional effective shear stress acting on the bed will be lower than the total Shields stress at bankfull flow. However, relative roughness (D_{50}/h_{bf}) does not differ significantly between West Coast and Other channels (Welch's t test for unequal variance, $P = 0.58$), suggesting that form drag due to grains is not responsible for the observed patterns in τ^*_{bf}/τ^*_c (Fig. S2). In-channel wood volumes, which may contribute substantially to hydraulic roughness, vary by orders of magnitude between channels (24), land management types, and biomes (31). Fig. 4*A* shows the effects of in-channel wood for a subset of our data. Even in West Coast channels devoid of wood, τ^*_{bf}/τ^*_c is substantially greater than 1. So, although high wood loading does have the expected effect of increasing τ^*_{bf}/τ^*_c (Fig. 4*A*), the form roughness associated with in-channel wood cannot alone explain the high τ^*_{bf}/τ^*_c observed in West Coast channels.

Bank cohesion from vegetation has been suggested as a driver of high τ^*_{bf}/τ^*_c (4). However, reanalyzing data used by Parker and others (4), we find no statistically significant difference in τ^*_{bf}/τ^*_c between bank vegetation classes (Fig. 4*B*). Although bank cohesion may not drive high values of τ^*_{bf}/τ^*_c, cohesion is nevertheless fundamentally important to maintaining stable banks under high τ^*_{bf}/τ^*_c conditions. In the absence of cohesion, the alluvial material making up channel banks should become unstable when $\tau^*_{bf} > 1.2\tau^*_c$ (7), leading to channel widening, which would, in turn, reduce flow depth and bed shear stress. However, fine sediment and vegetation provide cohesion on the banks of many natural channels. In small and midsized channels, where the magnitude of shear stress acting on the banks is moderate, vegetation can act to stabilize otherwise mobile banks (32). The prevalence of meandering gravel-bedded rivers provides further evidence that cohesive banks are common, as stable meander formation requires bank cohesion (33). In the presence of stable banks, physical experiments suggest that changes in bed surface texture can accommodate a fourfold change in sediment supply before aggradation begins (14). Thus, bank cohesion, although likely not responsible for driving increases in τ^*_{bf}/τ^*_c, is likely required to stabilize the banks of above-threshold channels.

It could be argued that West Coast channels, even the alluvial-bedded ones included in this study, may have more exposed bedrock and therefore should not conform to threshold channel assumptions. However, in low sediment supply settings, bedrock channels, like their alluvial counterparts, conform to $\tau^*_{bf} \approx \tau^*_c$ (8). Even in tectonically active channels that incise bedrock, the combined stress needed to move and transport sediment is typically much greater than the stress needed to incise rock (34). The stress required to incise rock is especially small where bedrock has low tensile strength, as in the case of the young sedimentary rocks that cover much of the West Coast. For example, modeling suggests that ~50% of the total bankfull shear stress along the South Fork Eel River in northern California is associated with the need to transport sediment and ~40% is related to initiating sediment motion (34). Hence, the distinction between channels that incise rock and those

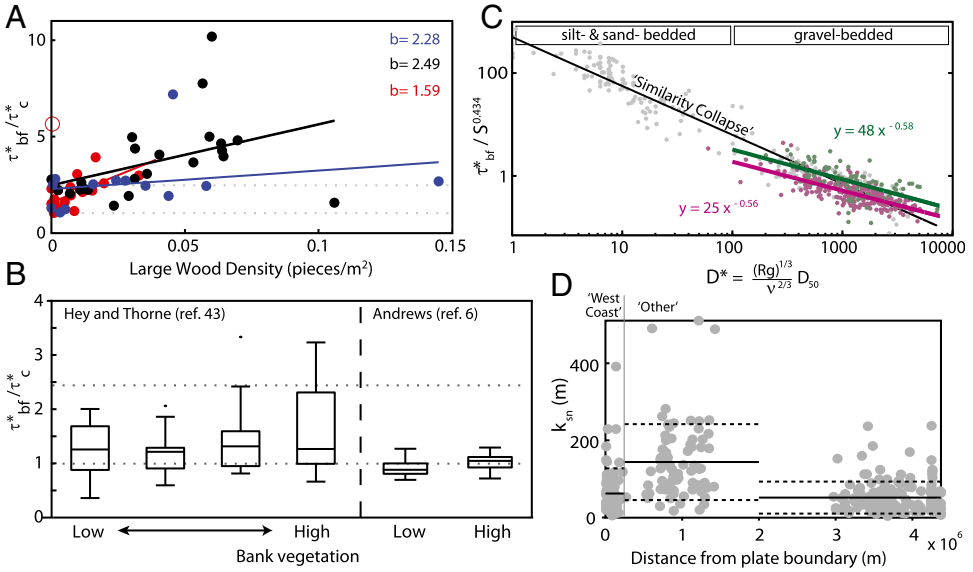

Fig. 4. Exploring alternative explanations for high τ^*_{bf}/τ^*_c. (*A*) The τ^*_{bf}/τ^*_c as a function of large wood density, separated by subregion. Olympic Peninsula (Washington) sites are in blue, Southeast Alaska sites are in black, and Middle Fork Salmon River (Idaho) sites are in red. The site marked with an open circle was excluded from the regression. The y-intercept values (b) from linear regressions are shown in colored text. (*B*) Effects of bank cohesion on τ^*_{bf}/τ^*_c. There are no statistically significant differences between bank vegetation classes within either dataset (ANOVA, ref. 43, $P = 0.15$; ref. 6, $P = 0.14$). In *A* and *B*, the upper and lower dashed gray lines mark the median τ^*_{bf}/τ^*_c ratio for West Coast and Other sites, respectively. (*C*) Overlay of our data compilation (in color) on the proposed (39) similarity collapse for all alluvial river data (greyscale). West Coast data and regression are in green, and Other are marked in maroon. The solid gray line denotes the best-fit regression through all alluvial river data shown by Li et al. (39), which is shown in gray. (*D*) Calculated normalized steepness (k_{sn}) plotted by distance from the plate boundary. Solid lines mark the means of each region; dotted lines mark 1 SD.

that simply convey sediment (i.e., alluvial channels) is neither clear nor necessarily useful in many settings.

Patterns in basin-averaged erosion rates are not reflected in continent-wide trends in normalized channel steepness (k_{sn}, *Materials and Methods* and Fig. 4*D*). According to the stream power model for river incision (35), we might expect channels actively incising uplifting rock to have high k_{sn} to match the high erosion rates (e.g., ref. 36). We do not observe concordance between k_{sn} and erosion rate at the continent scale (Figs. 1*D* and 4*D*). So, although k_{sn} may be strongly correlated with erosion rates within a region of similar climate and rock type (e.g., ref. 36), our results suggest that the relationship between grain size and channel geometry (τ^*_{bf}/τ^*_c or Q_t), rather than channel geometry and drainage area (k_{sn}), may be a more universal indicator of active tectonics, at least to the extent that it is correlated with coarse sediment supply.

We noted earlier that lithology affects the relationship between basin-wide erosion rates and coarse sediment supply. Rocks of low tensile strength will rapidly abrade during transport, yielding less bedload for a given sediment supply than their high tensile strength counterparts, thereby decreasing the coarse sediment supply felt by the bed of a gravel-bedded river. The τ^*_{bf}/τ^*_c data from the Oregon Coast Range nicely demonstrate this effect. During transport, Oregon Coast Range sedimentary rocks rapidly disintegrate into grain sizes that are transported as suspended load rather than bedload (21). So, although the erosion rates across the Oregon Coast Range are uniformly high [100 mm/ky to 200 mm/ky (16)], the channels sourcing Coast Range sedimentary rocks have remarkably little coarse sediment supply (21). The paucity of coarse sediment manifests in τ^*_{bf}/τ^*_c values below 1 (e.g., 0.37, 0.18). For lithology to explain the continent-wide trends in τ^*_{bf}/τ^*_c, West Coast basins would need to have substantially stronger bedrock. As a first-order test of the effect of lithology on our results, we determined the percent of basin area underlain by sedimentary rocks for sites in our compilation (*Basin Lithology* and Fig. S3). On average, there was little difference between West Coast and Other basins, which were underlain by 72% (SD 42%) and 72% (SD 39%) sedimentary bedrock, respectively. This would suggest that our data compilation does not oversample hard rocks on the West Coast, and lithology does not explain the continent-wide trends we observe. However, the effects of lithology are almost certainly important when comparing between individual basins (37) and likely drive scatter in Fig. 2.

The dependence of τ^*_{bf} on both slope (13, 23) and grain size can be used to produce a similarity collapse of all alluvial river data, including both bedload- and suspension-dominated systems (38). However, some scatter persists. Plotting our data compilation along the same axes used in the similarity collapse (39) (which are very nearly equivalent to plotting D_{50} on the horizontal axis and τ^*_{bf}/τ^*_c on the vertical), we see parallel trends in West Coast and Other channels, with West Coast channels having substantially higher τ^*_{bf} (Fig. 4*C*). To the extent that sediment supply drives the difference in trends between the two populations, we suggest that sediment supply is a major hidden variable driving the remaining scatter in the similarity collapse unifying all alluvial river morphology.

Many studies have called attention to the complexity of the incipient motion of grains in gravel-bedded rivers (13, 23). These studies imply that critical Shields stress should be viewed not as a constant but rather as a representative value used to generalize the stochastic process of grains being swept out of pockets by turbulent sweeps (40). Recent studies have shown that τ^*_c varies with channel slope (5, 23), grain packing geometry, and particle shape, among many other factors; thus, choices of τ^*_c should be made with these factors in mind (13). Similarly, we have shown here that bankfull channel geometry does not simply reflect the conditions required to initiate motion of D_{50}. Roughness, large wood loading, and bedrock exposure can affect τ^*_{bf}/τ^*_c, although our data suggest that these factors likely play a small role relative to sediment supply in driving the difference in τ^*_{bf}/τ^*_c between West Coast and Other channels. Rather, roughness, large wood loading, and bedrock exposure, along with flow intermittency (26) and local variability in characteristics such as bed material attrition (21) and uplift rate, likely help drive the scatter in τ^*_{bf}/τ^*_c that we observe within West Coast and Other channels, as well as the scatter about the trend in Fig. 2. We suggest that, as with τ^*_c, assumptions of constant τ^*_{bf}/τ^*_c must be made with caution.

Conclusions

In summary, our findings provide evidence that river channel hydraulic geometry and grain size are fundamentally linked to sediment supply. Threshold channels may therefore simply reflect settings with low sediment supplies. Because sediment transport rates are a highly nonlinear function of stress near the threshold for motion (3), small changes in stress result in large changes in transport capacity. Therefore, on the low end of the sediment supply spectrum, a relatively large range of sediment supply conditions may be accommodated with small changes in τ^*_{bf}/τ^*_c, giving the appearance that channel geometry is set by the critical stress. The observation that channels are, on average, adjusted to threshold conditions across much of the continent (8), may simply reflect the fact that most channels are subject to modest sediment supply. Although the average channel may conform to the threshold model, physically meaningful factors drive the scatter in τ^*_{bf}/τ^*_c. Our findings suggest that bankfull stresses can be, and are, maintained well above critical where sediment supplies are sufficiently high to require it. Bankfull Shields stress, bed surface armoring, and sediment supply are fundamentally linked in gravel-bedded rivers. Thus, an understanding of sediment supply is key to interpreting, predicting, or restoring bankfull hydraulic geometry in rivers.

Materials and Methods

Channel Geometry and Grain Size Data Compilation. To determine spatial patterns in bankfull Shields stress across North America, we compiled channel geometry and bed surface grain size data from 341 gravel-bedded river reaches with known locations (Dataset S1). We selected reaches with negligible regulation of flow and negligible sediment traps. Additionally, we chose reaches with primarily alluvial beds, and not immediately confined on both sides by bedrock banks. Our data are limited to gravel-bedded rivers, thus excluding the flatlands of the Great Plains where sand-bedded rivers predominate.

We calculated τ^*_{bf} (Eq. **1**) for each reach, substituting bankfull flow depth for hydraulic radius where bankfull width data were unavailable ($n = 7$). Because τ^*_c varies systematically with channel slope (5, 23), it would be misleading to compare τ^*_{bf} between reaches of different slope. Therefore, we normalize τ^*_{bf} by an estimated slope-dependent τ^*_c (23),

$$\tau^*_c = 0.15S^{0.25}. \quad [2]$$

For each site, we calculated the distance to the Pacific Plate boundary. Because portions of coastal California are west of the San Andreas Fault, and therefore could be considered a part of the Pacific Plate, we defined the plate boundary as the bathymetrically defined trench or the coast, whichever is farther west, thereby avoiding negative distance values. To compare West Coast sites with those elsewhere in North America, we use a threshold distance of 250 km from the Pacific Plate boundary.

Sediment Transport Capacity and Normalized Steepness. We use channel geometry and D_{50} to estimate bankfull sediment transport capacity per unit channel width, Q_t (square meters per second), for sites in the data compilation using the Recking (30) surface-based transport relation. The model, detailed in *Recking Sediment Transport Equations*, has been validated using independent field data from a variety of alluvial rivers. We note that sediment transport predictions, especially those based on just D_{50}, can substantially overpredict or underpredict sediment transport rates (41). However, our analysis relies on the observed trends in Q_t, not the precise values.

Sediment supply should equal sediment transport capacity in alluvial channels that are neither aggrading nor degrading. Thus, our prediction of sediment transport capacity can be viewed as a prediction of sediment supply.

In comparing Q_t to erosion rates, we rely on the assumption that the recurrence interval of bankfull flows is similar across most fluvial regimes (42). Although this is a simplification, we note that our dataset covers significant climate gradients across both latitude and longitude, complicating a snowpack or rainfall

intermittency explanation for observed patterns. Notably, a wide variety of hydrological environments are represented within the West Coast sites, from snowmelt-dominated streams to highly seasonal streams in Mediterranean climates.

For each of the sites, we calculate normalized steepness index [k_{sn} (meters)] assuming a reference concavity, θ, of 0.5 (35),

$$k_{sn} = SA^{\theta}. \quad [3]$$

Parker 1990 Model. The Parker (3) sediment transport model provides an independent prediction of the relationship between bed surface armoring, τ^*/τ^*_c, and sediment supply. We use the model to evolve Q_t and armor ratio from a given substrate grain size distribution and boundary shear stress (as in ref. 3, figure 4). For a detailed description, see *Parker Sediment Transport Model*.

We the use the Parker (3) model because it numerically describes the importance of bed surface armor in moderating the transport of different grain size fractions, and provides us with an independent prediction of the relationships we observe in our larger data compilation. The Parker model was originally written assuming that bed surface armor changes continuously throughout the flood hydrograph. In the intervening years, however, work has shown that armor very likely persists, invariant of flood stage (27, 28). In Fig. 3, we compare the modeled equilibrium armor ratios and transport capacities for a single channel at a variety of flood stages (τ^*/τ^*_c) to the bankfull conditions (τ^*_{bf}/τ^*_c) and armor ratio (measured at low flow conditions) of the natural rivers in our data compilation. Given the evolution in understanding since the original publication, we believe it is fair to compare the model results (equilibrium transport and armor at various flood stages) to our compilation of bankfull shear stresses and low flow observed armor.

ACKNOWLEDGMENTS. We thank T. Lisle, J. Buffington, C. Phillips, N. Snyder, and M. Cover for sharing databases of channel geometry and grain size measurements. This paper benefited from insightful conversations with M. Lamb, C. Phillips, and J. Pitlick, as well as constructive comments from the editor and two reviewers.

1. Dietrich WE, Kirchner JW, Ikeda H, Iseya F (1989) Sediment supply and the development of the coarse surface layer in gravel-bedded rivers. *Nature* 340(6230):215–217.
2. Mueller ER, Pitlick J (2013) Sediment supply and channel morphology in mountain river systems: 1. Relative importance of lithology, topography, and climate. *J Geophys Res Earth Surf* 118(4):2325–2342.
3. Parker G (1990) Surface-based bedload transport relation for gravel rivers. *J Hydraul Res* 28:417–436.
4. Parker G, Wilcock PR, Paola C, Dietrich WE, Pitlick J (2007) Physical basis for quasi-universal relations describing bankfull hydraulic geometry of single-thread gravel bed rivers. *J Geophys Res* 112(F4):F04005.
5. Mueller ER, Pitlick J, Nelson JM (2005) Variation in the reference Shields stress for bed load transport in gravel-bed streams and rivers. *Water Resour Res* 41(4):W04006.
6. Andrews E (1984) Bed-material entrainment and hydraulic geometry of gravel-bed rivers in Colorado. *Geol Soc Am Bull* 95:371–378.
7. Parker G (1978) Self-formed straight rivers with equilibrium banks and mobile bed. Part 2. The gravel river. *J Fluid Mech* 89(1):127–146.
8. Phillips CB, Jerolmack DJ (2016) Self-organization of river channels as a critical filter on climate signals. *Science* 352(6286):694–697.
9. Buffington JM, Montgomery DR (1997) A systematic analysis of eight decades of incipient motion studies, with special reference to gravel-bedded rivers. *Water Resour Res* 33(8):1993–2029.
10. Willenbring JK, Codilean AT, McElroy B (2013) Earth is (mostly) flat: Apportionment of the flux of continental sediment over millennial time scales. *Geology* 41(3):343–346.
11. Fernandez-Luque R, Van Beek R (1976) Erosion and transport of bed-load sediment. *J Hydraul Res* 14(2):127–144.
12. Buffington J, Montgomery D (1999) Effects of sediment supply on surface textures of gravel-bed rivers. *Water Resour Res* 35(11):3523–3530.
13. Bunte K, Abt SR, Swingle KW, Cenderelli DA, Schneider JM (2013) Critical Shields values in coarse-bedded steep streams. *Water Resour Res* 49(11):7427–7447.
14. Eaton BC, Church M (2009) Channel stability in bed load-dominated streams with nonerodible banks: Inferences from experiments in a sinuous flume. *J Geophys Res Earth Surf* 114(F1):F01024.
15. Madej MA, Sutherland DG, Lisle TE, Pryor B (2009) Channel responses to varying sediment input: A flume experiment modeled after Redwood Creek, California. *Geomorphology* 103(4):507–519.
16. Balco G, Finnegan N, Gendaszek A, Stone JOH, Thompson N (2013) Erosional response to northward-propagating crustal thickening in the coastal ranges of the U.S. Pacific Northwest. *Am J Sci* 313(8):790–806.
17. Matmon A, et al. (2003) Temporally and spatially uniform rates of erosion in the southern Appalachian Great Smoky Mountains. *Geology* 31(2):155–158.
18. Ganti V, et al. (2016) Time scale bias in erosion rates of glaciated landscapes. *Sci Adv* 2(10):e1600204.
19. Kirchner JW, et al. (2001) Mountain erosion over 10 yr, 10 k.y., and 10 m.y. time scales. *Geol Soc Am Bull* 29(7):591–594.
20. Reusser L, Bierman P, Rood D (2015) Quantifying human impacts on rates of erosion and sediment transport at a landscape scale. *Geology* 43(2):171–174.
21. O'Connor JE, et al. (2014) Geologic and physiographic controls on bed-material yield, transport, and channel morphology for alluvial and bedrock rivers, western Oregon. *Bull Geol Soc Am* 126(3-4):377–397.
22. Turowski JM, Rickenmann D, Dadson SJ (2010) The partitioning of the total sediment load of a river into suspended load and bedload: A review of empirical data. *Sedimentology* 57(4):1126–1146.
23. Lamb MP, Dietrich WE, Venditti JG (2008) Is the critical Shields stress for incipient sediment motion dependent on channel-bed slope? *J Geophys Res* 113(F2):F02008.
24. Buffington J, Montgomery D (1999) Effects of hydraulic roughness on surface textures of gravel-bed rivers. *Water Resour Res* 35(11):3507–3521.
25. Mark DM, Church M (1977) On the misuse of regression in earth science. *Math Geol* 9(1):63–75.
26. Hassan MA, Egozi R, Parker G (2006) Experiments on the effect of hydrograph characteristics on vertical grain sorting in gravel bed rivers. *Water Resour Res* 42(9):1–15.
27. Wilcock PR, DeTemple BT (2005) Persistence of armor layers in gravel-bed streams. *Geophys Res Lett* 32(8):L08402.
28. Parker G, Hassan M, Wilcock P (2006) Adjustment of the bed surface size distribution of gravel-bed rivers in response to cycled hydrographs. *Gravel-Bed Rivers VI: From Process Understanding to River Restoration*, eds Habersack H, Pieglay H, Rinaldi M (Elsevier, New York), pp 1–46.
29. Parker G, Klingeman P (1982) On why gravel bed streams are paved. *Water Resour Res* 18(5):1409–1423.
30. Recking A (2013) Simple method for calculating reach-averaged bed-load transport. *J Hydraul Eng* 139(1):70–75.
31. Benda L, Bigelow P (2014) On the patterns and processes of wood in northern California streams. *Geomorphology* 209:79–97.
32. Eaton BC, Giles TR (2008) Assessing the effect of vegetation-related bank strength on channel morphology and stability in gravel-bed streams using numerical models. *Earth Surf Processes Landforms* 34(5):712–724.
33. Braudrick CA, Dietrich WE, Leverich GT, Sklar LS (2009) Experimental evidence for the conditions necessary to sustain meandering in coarse-bedded rivers. *Proc Natl Acad Sci USA* 106(40):16936–16941.
34. Sklar LS, Dietrich WE (2008) Implications of the saltation–abrasion bedrock incision model for steady-state river longitudinal profile relief and concavity. *Earth Surf Processes Landforms* 1151:1129–1151.
35. Whipple KX (2004) Bedrock rivers and the geomorphology of active orogens. *Annu Rev Earth Planet Sci* 32(1):151–185.
36. DiBiase RA, Whipple KX, Heimsath AM, Ouimet WB (2010) Landscape form and millennial erosion rates in the San Gabriel Mountains, CA. *Earth Planet Sci Lett* 289(1-2):134–144.
37. Mueller ER, Smith ME, Pitlick J (2016) Lithology-controlled evolution of stream bed sediment and basin-scale sediment yields in adjacent mountain watersheds, Idaho, USA. *Earth Surf Processes Landforms* 1883:1869–1883.
38. Li C, Czapiga MJ, Eke EC, Viparelli E, Parker G (2014) Variable Shields number model for river bankfull geometry: bankfull shear velocity is viscosity-dependent but grain size-independent. *J Hydraul Res* 1686(1):1–13.
39. Li C, Czapiga MJ, Eke EC, Viparelli E, Parker G (2016) Closure to "Variable Shields number model for river bankfull geometry: Bankfull shear velocity is viscosity-dependent but grain size-independent." *J Hydraul Res* 54(2):234–237.
40. Kirchner JW, Dietrich WE, Iseya F, Ikeda H (1990) The variability of critical shear stress, friction angle, and grain protrusion in water worked sediments. *Sedimentology* 37:647–672.
41. Gomez B, Church M (1989) An assessment of bed load sediment transport formulae for gravel bed rivers. *Water Resour Res* 25(6):1161–1186.
42. Leopold LB, Wolman MG, Miller JP (1964) *Fluvial Processes in Geomorphology* (W. H. Freeman, New York).
43. Hey R, Thorne C (1986) Stable channels with mobile gravel beds. *J Hydraul Eng* 112:671–689.
44. Garrity CP, Soller DR (2009) *Database of the Geologic Map of North America; Adapted from the Map by J.C. Reed, Jr. and Others (2005)* (US Geol Surv, Boulder, CO), Data Ser 424. Available at https://pubs.usgs.gov/ds/424/. Accessed November 2016.
45. Friedman GM (1987) Vertical movements of the crust: Case histories from the northern Appalachian Basin. *Geology* 15:1130–1133.
46. Parker G, Klingeman PC, McLean DL (1982) Bedload and size distribution in paved gravel bed streams. *J Hydraul Div ASCE* 108:544–571.

Supporting Information

Pfeiffer et al. 10.1073/pnas.1612907114

Basin Lithology

Using a geologic map of North America (44), a 15-arc-second digital elevation model, and a digital stream network (https://hydrosheds.cr.usgs.gov/), we extract basin lithology data for each basin in our data compilation, from which we calculate the percent of each basin underlain by sedimentary rock. We use percent sedimentary bedrock as a rough measure of the influence of lithology on the ratio of bedload to suspended load in our data compilation, as sedimentary rocks tend to abrade most rapidly (21). We note that the sedimentary rocks of the Appalachian Basin have undergone diagenesis during burial and exhumation from depths of >5 km (45), which tends to make them stronger than the younger sedimentary rocks of the West Coast. Thus, the comparison of lithologic effects between West Coast and Other sites is conservative, as sedimentary rocks on the West Coast will tend to more rapidly abrade into suspended load, decreasing the effective coarse sediment supply for a given erosion rate. Because a 15-arc-second grid imperfectly captures basin geometry, especially for smaller basins, we checked the output drainage areas against the drainage areas reported in the source literature. We discarded any basins with a mismatch in drainage area of >15%, unless it was clear from visual inspection of the source data that the basin was underlain entirely by one lithologic category. In total, we retained 51 West Coast sites and 156 sites on the rest of the continent for our lithologic analysis.

Recking Sediment Transport Equations

We use channel geometry and grain size data to estimate volumetric bankfull sediment transport capacity per unit channel width, Q_t (square meters per second), for sites in our data compilation using the Recking (30) surface-based transport relation. These transport estimates appear in Fig. 3 (colored points) and in Fig. S1. The Recking equations are well suited to our purposes because they are designed specifically for situations in which data on channel grain size are limited (e.g., incomplete knowledge of the surface, subsurface, or bedload grain size distribution), as is the case in our data compilation. Secondly, in this model, Q_t is not a function of excess bed surface shear stress (i.e., τ^*_{bf}-τ^*_c) but instead assumes partial mobility at low-to-moderate flows. Thus, with the knowledge of only channel slope (S), bankfull width [w (meters)], bankfull depth [h (meters)], and median bed surface grain size [D_{50} (meters)], we can predict nonzero transport even in channels where τ^*_{bf}-$\tau^*_c < 1$.

Recking frames transport in terms of the mobility of the 84th percentile bed surface grain size, D_{84}. Lacking knowledge of D_{84} for most of our sites, we follow the suggestion of Recking and estimate D_{84} from D_{50},

$$D_{84} = 2.1 D_{50}. \quad \text{[S1]}$$

Recking approximates the Shields stress corresponding to the transition from partial to full mobility of the bed surface grains as

$$\tau^*_m = (5S + 0.06)\left(\frac{D_{84}}{D_{50}}\right)^{4.4\sqrt{S}-1.5}. \quad \text{[S2]}$$

The bankfull Shields stress associated with D_{84} is

$$\tau^*_{84} = \frac{S\, R_{bf}}{(s-1)D_{84}}, \quad \text{[S3]}$$

where s is the relative density of the sediment (ρ_s/ρ), for which we assume a value of 2.65.

Using τ^*_m and τ^*_{84}, Recking approximates the dimensionless sediment discharge, q^*, as

$$q^* = \frac{14\ \tau^{*\,2.5}_{84}}{\left[1 + \left(\tau^*_m/\tau^*_{84}\right)^4\right]}, \quad \text{[S4]}$$

from which we calculate the volumetric sediment flux per unit width (square meters per second),

$$Q_t = \sqrt{(s-1)gD^3_{84}}\,q^*, \quad \text{[S5]}$$

where g is the gravitational constant.

Parker Sediment Transport Model

Parker (3) presents a transformation from the subsurface-based relation of Parker et al. (46) to a sediment transport model based on the grain size distribution of the bed surface. Using the equations presented in his transformation, we can relate the transport stage $\tau*/\tau^*_c$ to both bed surface armoring (D_{50}/D_{50ss}) and sediment flux, Q_t. These data are presented in the colored curve in Fig. 4. We note that we are not using the final surface-based transport relation to determine these values, but rather are using the intermediate equations in ref. 3. We calculate Q_t based on the subsurface grain size distribution, then determine the surface grain size distribution (and therefore, armor ratio) from the equations derived by Parker (3) as a part of the subsurface-to-surface transformation. Below, we use notation that is consistent with that used above and in the main manuscript, not the notation used by Parker, although we provide the original equation numbers from ref. 3.

Our goal is to predict the bed surface armor ratio (D_{50}/D_{50ss}) and sediment flux (Q_t) for an example river at a variety of transport stages τ^*/τ^*_c. As inputs for the model, we used the Oak Creek channel slope, S, and subsurface grain size distribution, as in ref. 3. The subsurface grain size distribution is broken into n size classes, each of which is described by its diameter, D_i, and fraction of the total subsurface grain size distribution, f_i.

We used the following steps for a range of substrate-based transport stages (ϕ_{50}) (ref. 3, equation 4a):

$$\phi_{50} = \tau^*_{ss}/\tau^*_{rss}, \quad \text{[S6]}$$

where the subsurface Shields stress, τ^*_{ss}, is (ref. 3, equation 4b)

$$\tau^*_{ss} = \tau/(\rho_s\text{-}\rho)gD_{50ss}, \quad \text{[S7]}$$

and τ^*_{rss} is a reference Shields stress associated with the mobility of D_{50ss} with an assumed value of 0.0876. Ultimately, we transform these ϕ_{50} values to the surface-based transport stage ϕ_{sg0} (nearly equivalent to τ^*/τ^*_c) for display in Fig. 4.

For each ϕ_{50}, we determine the substrate-based transport stage associated with each individual grain size fraction (f_i),

$$\phi_i = g_{si}\phi_{50}, \quad \text{[S8]}$$

using the substrate-based hiding function (g_{si}) (ref. 3, equation 11),

$$g_{si} = 1.048(D_i/D_{50ss})^{-0.0951}. \quad \text{[S9]}$$

For each ϕ_i, we determine the dimensionless bedload transport rate (W^*_i) according to Parker (ref. 3, equation 13),

$$W_i^* = 0.00218 G_i, \quad \textbf{[S10]}$$

in which G_i is the piecewise empirical transport function (ref. 3, equation 5),

$$G_i = \begin{cases} 5474\left(1 - \dfrac{0.853}{\phi_i}\right)^{4.5} & \phi_i > 1.59 \\ \exp\left[14.2(\phi_i - 1) - 9.28(\phi_i - 1)^2\right] & 1 \le \phi_i \le 1.59 \\ \phi_i^{14.2} & \phi_i < 1 \end{cases}. \quad \textbf{[S11]}$$

The total dimensionless bedload transport rate across all grain size fractions for the given ϕ_{50} is then

$$W_{\text{tot}}^* = \sum_{i=1}^{n} W_i^*. \quad \textbf{[S12]}$$

The dimensionless transport rate is then converted to a volumetric sediment transport rate per unit channel width, Q_t (square meters per second) (ref. 3, equation 7b),

$$Q_t = W_{\text{tot}}^* (\tau/\rho)^{3/2} \Big/ \text{Rg}. \quad \textbf{[S13]}$$

R is the submerged specific gravity of sediment $[(\rho_s - \rho)/\rho]$, assumed to be 1.65. The bed surface shear stress, τ (newtons per square meter), can be obtained by combining and rearranging Eqs. S6 and **S7**, above,

$$\tau = \phi_{50} \tau_{\text{rss}}^* (\rho_s\text{-}\rho) g D_{50\text{ss}}. \quad \textbf{[S14]}$$

To determine the surface median grain size, D_{50}, we first solve for the surface grain size distribution, which is described as grain size fractions, F_i, using the same diameter bins, D_i, as above (ref. 3, equation 12a),

$$F_i = (f_i/G_i) G_{\text{tot}}, \quad \textbf{[S15]}$$

where G_{tot} is a metric of the total bedload transport for all grain size fractions (ref. 3, equation 12b)

$$G_{\text{tot}} = \frac{1}{\sum_{i=1}^{n} f_i/G_i}. \quad \textbf{[S16]}$$

Using the calculated bed surface grain size fractions, we determine the surface median grain size (ref. 3, equation 14),

$$D_{50} = e^{\sum_{i=1}^{n} F_i \ln D_i}, \quad \textbf{[S17]}$$

from which we calculate the armor ratio $D_{50}/D_{50\text{ss}}$.

Because we want to compare armor and Q_t to a surface-based measure of transport stage, i.e., τ^*/τ_c^*, rather than to a substrate-based one (ϕ_{50}), we calculate ϕ_{sg0}, the surface-based transport stage associated with D_{50}, for each case of ϕ_{50} according to (ref. 3, equation 17a)

$$\phi_{\text{sg0}} = \tau_{\text{sg}}^* / \tau_{\text{rsg0}}^*, \quad \textbf{[S18]}$$

where the surface-based Shields stress, τ_{sg}^*, and the reference surface-based Shields stress, τ_{rsg0}^*, are (ref. 3, equation 17b)

$$\tau_{\text{sg}}^* = \tau/(\rho_s\text{-}\rho) g D_{50} \quad \textbf{[S19]}$$

and (ref. 3, equation 19)

$$\tau_{\text{rsg0}}^* = 0.0386. \quad \textbf{[S20]}$$

We note that, when we compare the output of the Parker model to our data in Fig. 3, we are equating the surface-based reference Shields stress (τ_{rsg0}^*) to the critical Shields stress (τ_c^*). These two values are very nearly similar. Additionally, we equate the surface-based Shields stress (τ_{sg}^*) to the bankfull Shields stress (τ_{bf}^*). For a discussion of this comparison, see *Materials and Methods*.

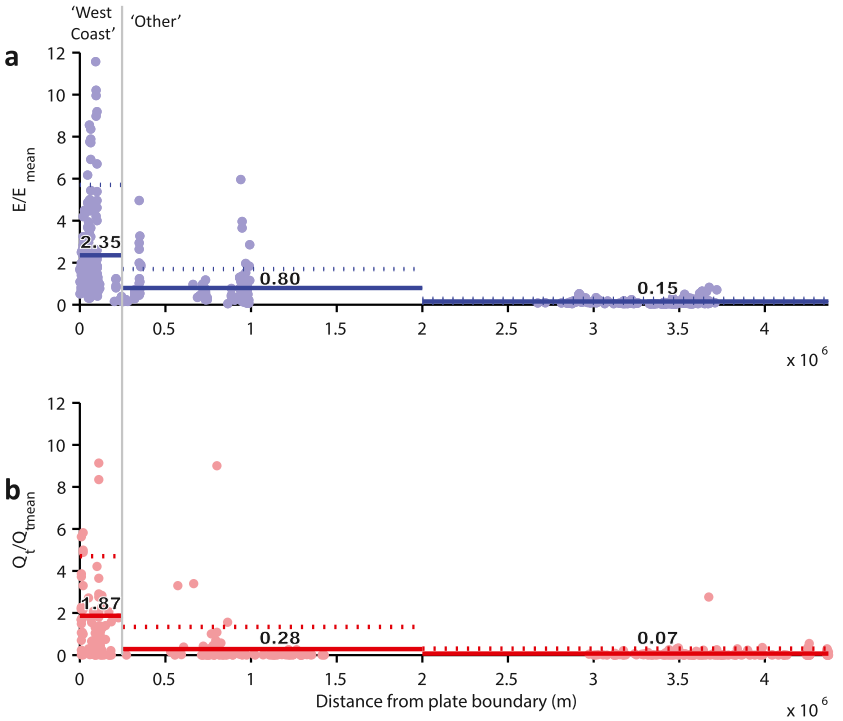

Fig. S1. Transport capacity and erosion rate (E) away from the Pacific Plate boundary. (*A*) Erosion rate as a proportion of mean erosion rate and (*B*) calculated sediment transport capacity as a proportion of mean sediment transport capacity plotted by distance from the plate boundary. Solid lines mark the means of each region, and dotted lines mark 1 SD. Means for each region are marked in black text. Three high E and one high Q_t points, all within the West Coast region, plot off the axes. Sespe Creek, CA, and Fish Creek, AK, with Q_t/Q_{tmean} of 93 and 36, respectively, plot above the axes.

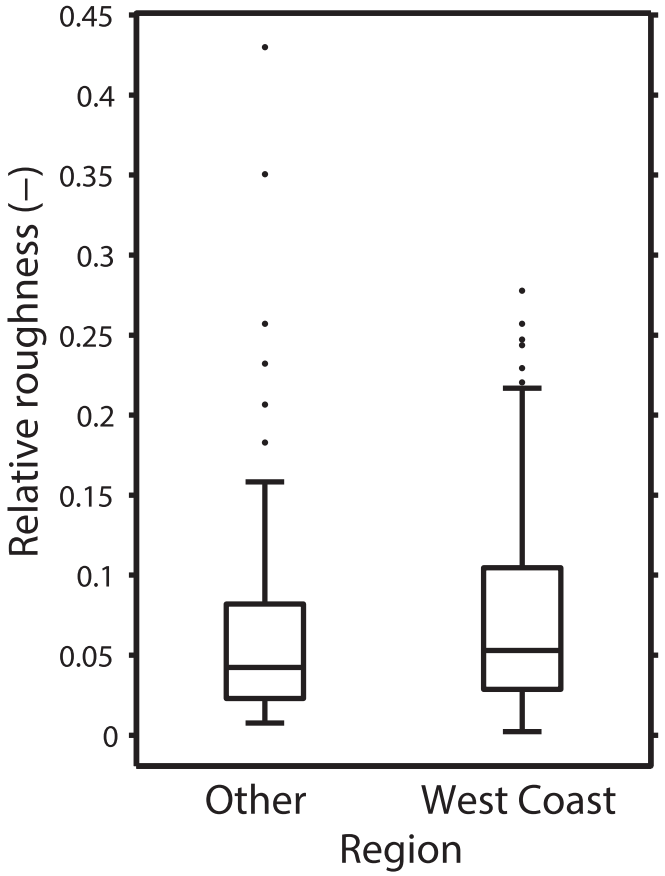

Fig. S2. Boxplot of relative roughness (D_{50}/h) measured at each site in the data compilation, separated by region.

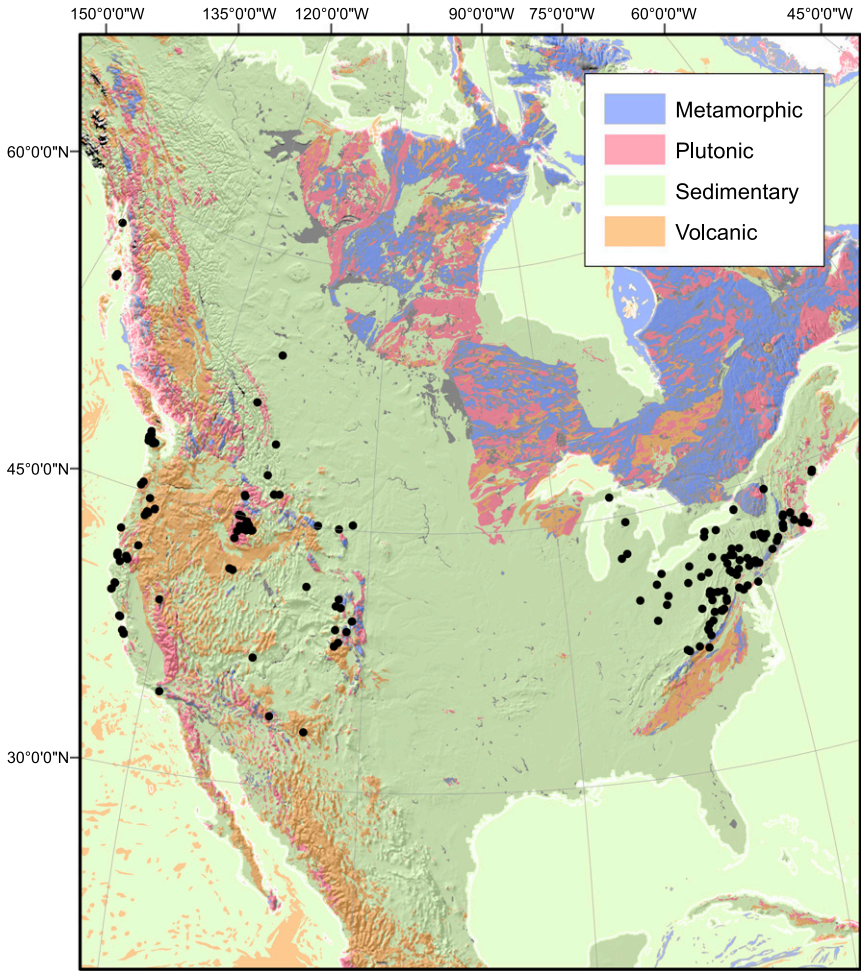

Fig. S3. Shaded relief model overlain by the US Geological Survey Geologic Map of North America, separated into broad lithologic categories. Black dots mark the location of sites within our data compilation for which we calculated percent sedimentary bedrock. Lithology data from ref. 44.

Other Supporting Information Files

Dataset S1 (TXT)
Dataset S2 (TXT)